

Article

Synchrosqueezing Transform Based on Frequency-Domain Gaussian-Modulated Linear Chirp Model for Seismic Time–Frequency Analysis

Pingping Bing ^{1,*}, Wei Liu ², Haoqi Zhang ¹, Li Zhu ¹, Guiping Zhu ¹, Jun Zhou ¹ and Binsheng He ^{1,*}

¹ Hunan Provincial Key Laboratory of the Research and Development of Novel Pharmaceutical Preparations, Changsha Medical University, Changsha 410219, China

² College of Mechanical and Electrical Engineering, Beijing University of Chemical Technology, Beijing 100029, China; liuwei_upc@126.com

* Correspondence: bpping@163.com (P.B.); hbcsmu@163.com (B.H.)

Abstract: The synchrosqueezing transform (SST) has attracted much attention as a post-processing technique since it was proposed. In recent years, improvements to SST have been made. However, the existing methods are mainly based on the time-domain signal model, and the weak frequency modulation assumption for the components composing the signal is always taken into account. Thus, the signals characterized by a rapidly changing instantaneous frequency (IF) may fail to be adequately tackled. To address this problem, the paper presents a novel seismic time–frequency analysis method via synchrosqueezing transform where a frequency-domain Gaussian modulated linear chirp model is utilized to deduce the SST. The group delay (GD) rather than the IF estimator is implemented to compute an estimation of the ridge. Furthermore, a new synchrosqueezing operator is constructed to rearrange the energy around the ridge. A synthetic example verifies the efficiency and robustness of the proposed SST method, which generates better results than some classic time–frequency analysis (TFA) approaches, e.g., short-time Fourier transform (STFT) and STFT-based SST (FSST). A field dataset further demonstrates this method’s potential in the delineation of subsurface geological structures.

Keywords: time–frequency representation; synchrosqueezing transform; chirp model; time localization; geological structures

MSC: 86-10



Citation: Bing, P.; Liu, W.; Zhang, H.; Zhu, L.; Zhu, G.; Zhou, J.; He, B. Synchrosqueezing Transform Based on Frequency-Domain Gaussian-Modulated Linear Chirp Model for Seismic Time–Frequency Analysis. *Mathematics* **2023**, *11*, 2904. <https://doi.org/10.3390/math11132904>

Academic Editors: Valentina Yakovleva and Roman Parovik

Received: 30 May 2023
Revised: 21 June 2023
Accepted: 25 June 2023
Published: 28 June 2023



Copyright: © 2023 by the authors. Licensee MDPI, Basel, Switzerland. This article is an open access article distributed under the terms and conditions of the Creative Commons Attribution (CC BY) license (<https://creativecommons.org/licenses/by/4.0/>).

1. Introduction

In the real world, nonstationary signals exist widely in different forms, such as seismic waves, radar signals, and communications and sonar systems [1–5]. Time–frequency analysis (TFA) is a powerful tool for the analysis of nonstationary signals when a one-dimensional signal of time can be mapped into a two-dimensional signal of time and frequency, which makes it feasible to characterize the time–frequency information [6]. The most common time–frequency analysis algorithms are the short-time Fourier transform (STFT) [7] and continuous wavelet transform (CWT) [8]. However, because of the Heisenberg uncertainty principle, such transforms fail to obtain a satisfactory time–frequency representation (TFR) result. In addition, the STFT is more affected by different types of window functions, and the width of the window function directly relates to the time–frequency resolution. Despite the variable resolution by means of a wavelet family, the CWT cannot enhance time and frequency resolutions simultaneously [9–11]. The Wigner–Ville distribution (WVD) [12], a quadratic algorithm, improves the readability of a TFR by concentrating the energy density in the time–frequency plane, but the cross-terms that exist in the energy distribution of the WVD when coping with multicomponent signals hinder its further application in practice.

In order to solve these issues, many efforts have been made. Auger and Flandrin [13] introduced a post-processing approach called the reassignment method (RM) to sharpen the TFR where it achieves the reassignment of time–frequency transformation coefficients along the two axes of time and frequency using the time and frequency derivatives of its phase. Unfortunately, the RM is not invertible; that is, the modes cannot be reconstructed from the TFR. To this end, Daubechies et al. [14] proposed an alternative solution called synchrosqueezing transform (SST), which was first used in audio signal processing [15]. This method is based on a wavelet framework and has a reasonable theoretical principle. Moreover, the SST is capable of enhancing the readability of TFR and is characterized by the invertible property [16,17]. Thakur and Wu [18] developed the STFT-based SST (FSST) by extending the ‘synchrosqueezing’ idea to the STFT framework. Nevertheless, it should be noted that both methods, SST and FSST, need to satisfy the assumption that the components that make up the signal are weakly frequency-modulated, which indicates that the signals characterized by a rapidly changing instantaneous frequency (IF) are unable to be adequately handled. Recently, Oberlin et al. [19] utilized a second-order estimate of the IF to enhance the mode reconstruction and localization processes based on an SST framework; this is called second-order synchrosqueezing transform (FSST2). Afterward, Duong-Hung Pham and Sylvain Meignen [20] generalized the FSST2 to an N-order SST (FSSTN), namely a high-order synchrosqueezing transform, by implementing high-order approximations on the amplitude and phase of the signal [21]. Liu et al. [22] employed a three-parameter S transform (TPST) to control the window width in order to optimize the time–frequency resolution flexibly and applied it to detect the channels and characterize the channel features. Li et al. [23] proposed the time-synchroextracting transform (TSET) for the delineation of subsurface geological information, which achieves a highly concentrated time–frequency representation for the signal with a rapidly varying instantaneous frequency. Bing et al. [24] presented a seismic time–frequency analysis method based on a time-reassigned synchrosqueezing transform (TSST) to highlight subtle geological structures, where the time–frequency coefficients are reassigned in the time direction rather than in the frequency direction. Yu et al. [25] developed a high-resolution processing technique for the detection of seismic activities in gas reservoirs and carried out identification using the improved synchrosqueezing transform, which only adjusts the phase of the signal before and after transformation. Paksima et al. [26] analyzed the capabilities of a high-resolution synchrosqueezing S-transform on nonstationary seismic signals and used it to describe the gas accumulation zones and accurately separate two different gas reservoir formations based on enhanced resolution in both time and frequency directions.

It is worth noting that all above-mentioned synchrosqueezing methods use a time-domain signal model; the IF is computed by the partial derivative of the instantaneous phase with respect to the time, and then the estimated IF is utilized to sharpen the TFR along the frequency or time direction. In this paper, we propose a novel seismic time–frequency analysis method via synchrosqueezing transform where a frequency-domain Gaussian-modulated linear chirp model is employed to deduce the SST, and, inspired by the FSST2, we extend the frequency-domain SST to the second-order version, which is more suited to analyze signals characterized by a strongly changing IF. In this method, the traditional IF estimator based on the instantaneous phase is replaced by the group delay (GD) to compute an estimation of the ridge. Then, a new synchrosqueezing operator is constructed to rearrange the energy around the ridge along the horizontal direction. The key contributions of this paper are summarized as follows:

- (1) We construct a new synchrosqueezing operator to rearrange the time–frequency energy along the time direction.
- (2) We first investigate the properties of SST and second-order SST in the frequency domain and achieve seismic time–frequency feature extraction;
- (3) The proposed method shows a large advantage over conventional STFT and FSST approaches in characterizing subtle geological structures.

The organization of this paper is arranged as follows. We first review some fundamental notations and definitions of the Fourier transform and STFT in Section 2. Then, we introduce a frequency-domain Gaussian modulated linear chirp model and the GD estimation to deduce the new SST and second-order SST. Sections 3 and 4 show several examples concerning a synthetic signal and a field dataset and compare the proposed approach with some classical techniques, such as STFT and FSST. This comparison validates the effectiveness of the proposed method in time localization and the description of subsurface geological structures. Section 5 provides some discussions on this subject. Finally, the conclusions are presented in Section 6.

2. Methodology

2.1. Theoretical Basis

For a signal $f(t)$, the Fourier transform is formulated as

$$F(\zeta) = \int_{-\infty}^{+\infty} f(t)e^{-i2\pi\zeta t} dt \tag{1}$$

where t is the time variable and ζ is the frequency variable.

The Fourier spectrum $F(\zeta)$ depicts the frequency information of the signal $f(t)$ over the entire time; however, it is not appropriate to analyze a nonstationary signal using only the expression in the time or frequency domain. Consequently, the STFT was introduced, and the STFT of the above signal $f(t)$ is defined as

$$V_f^g(t, \zeta) = \int_{-\infty}^{+\infty} f(\tau)g^*(\tau - t)e^{-i2\pi\zeta\tau} d\tau \tag{2}$$

where g^* denotes the complex conjugate of a window function g .

According to Parseval's theorem, the frequency-domain STFT can be expressed as

$$\begin{aligned} V_f^g(t, \zeta) &= V_f^G(t, \zeta) \\ &= \frac{1}{2\pi} \int_{-\infty}^{+\infty} F(\xi)G^*(\xi - \zeta)e^{i2\pi t(\xi - \zeta)} d\xi \end{aligned} \tag{3}$$

where $F(\xi)$ and $G(\zeta)$ are Fourier transforms of signal f and window function g , respectively. Note that we abbreviate $V_f^G(t, \zeta)$ as V_f^G in the following equations for convenience, Appendix A.

Additionally, the inverse Fourier transform can be implemented to reconstruct the original signal $f(t)$ on the condition that $G(\zeta)$ does not vanish and is continuous at zero, Appendix B.

$$f(t) = F^{-1}\left(\frac{1}{G^*(0)} \int_{-\infty}^{+\infty} V_f^G dt\right) \tag{4}$$

2.2. Frequency-Domain SST (FDSST)

A Gaussian-modulated linear chirp signal model in the frequency domain is considered as follows:

$$F(\zeta) = A(\zeta)e^{i2\pi\psi(\zeta)} \tag{5}$$

where $F(\zeta)$ is the Fourier transform of the analyzed signal $f(t)$, and $A(\zeta)$ and $\psi(\zeta)$ denote the amplitude function and phase function, respectively.

Then, the GD can be written as

$$\tau(\zeta) = -\frac{d\psi(\zeta)}{d\zeta} \tag{6}$$

The core idea of frequency-domain SST is to improve the TFR using a new reassignment operator $\tilde{v}_f(t, \zeta)$, which is defined as ($V_f^G(t, \zeta) \neq 0$), such that

$$\tilde{v}_f(t, \zeta) = -\frac{\partial_\zeta V_f^G(t, \zeta)}{i2\pi V_f^G(t, \zeta)} \tag{7}$$

where

$$\begin{aligned} & \partial_\zeta V_f^G(t, \zeta) \\ = & -\frac{1}{2\pi} \int_{-\infty}^{+\infty} F(\xi) [G^*(\xi - \zeta)]' e^{i2\pi t(\xi - \zeta)} d\xi \\ & - i2\pi t \frac{1}{2\pi} \int_{-\infty}^{+\infty} F(\xi) G^*(\xi - \zeta) e^{i2\pi t(\xi - \zeta)} d\xi \\ = & -V_f^{G'}(t, \zeta) - i2\pi t V_f^G(t, \zeta) \end{aligned} \tag{8}$$

Thus, the real part of $\tilde{v}_f(t, \zeta)$, namely $\hat{v}_f(t, \zeta) = R[\tilde{v}_f(t, \zeta)]$, denotes the estimated GD. Finally, the frequency-domain SST is expressed as

$$T_f^{G,\gamma}(t, \zeta) = \frac{1}{G^*(0)} \int_{\{t, |V_f^G| > \gamma\}} V_f^G(\mu, \zeta) \delta(t - \hat{v}_f(\mu, \zeta)) d\mu \tag{9}$$

where γ is the threshold.

Moreover, the original signal $f(t)$ can be reconstructed by an inverse Fourier transform.

$$f(t) = F^{-1} \left(\int_{-\infty}^{+\infty} T_f^{G,\gamma}(t, \zeta) dt \right) \tag{10}$$

where $F^{-1}(\bullet)$ denotes the inverse Fourier transform.

2.3. Frequency-Domain Second-Order SST (FDSST2)

Inspired by FSST2, a second-order local modulation operator is defined and employed to compute the new second-order local GD estimation.

For the signal $f(t)$, the reassignment operator $\tilde{\omega}_f(t, \zeta)$ is defined by ($V_f^G(t, \zeta) \neq 0$):

$$\tilde{\omega}_f(t, \zeta) = \zeta + \frac{\partial_t V_f^G(t, \zeta)}{i2\pi V_f^G(t, \zeta)} \tag{11}$$

where

$$\begin{aligned} \partial_t V_f^G(t, \zeta) &= \frac{1}{2\pi} \int_{-\infty}^{+\infty} F(\xi) G^*(\xi - \zeta) \\ & \quad \left(i2\pi(\xi - \zeta) e^{i2\pi t(\xi - \zeta)} \right) d\xi \\ &= i2\pi \frac{1}{2\pi} \int_{-\infty}^{+\infty} F(\xi) (\xi - \zeta) \\ & \quad G^*(\xi - \zeta) e^{i2\pi t(\xi - \zeta)} d\xi \\ &= i2\pi V_f^{\zeta G}(t, \zeta) \end{aligned} \tag{12}$$

Now, we combine Equations (7) and (11) to obtain the second-order modulated modulation operator $\tilde{q}_f(t, \zeta)$, namely,

$$\tilde{q}_f(t, \zeta) = \frac{\partial_t \tilde{v}_f(t, \zeta)}{\partial_t \tilde{\omega}_f(t, \zeta)} \quad \text{when } \partial_t \tilde{\omega}_f(t, \zeta) \neq 0 \tag{13}$$

Then, the second-order GD estimate of signal $f(t)$ is described as

$$\tilde{v}_f^{[2]}(t, \varsigma) = \begin{cases} \tilde{v}_f(t, \varsigma) + \tilde{q}_f(t, \varsigma) (\varsigma - \tilde{\omega}_f(t, \varsigma)) & \text{if } \partial_t \tilde{\omega}_f \neq 0 \\ \tilde{v}_f(t, \varsigma) & \text{otherwise} \end{cases} \quad (14)$$

Additionally, the estimated GD is written as

$$\hat{v}_f^{[2]}(t, \varsigma) = R \left[\tilde{v}_f^{[2]}(t, \varsigma) \right] \quad (15)$$

The frequency-domain second-order SST is defined by replacing $\hat{v}_f(\mu, \varsigma)$ with $\hat{v}_f^{[2]}(\mu, \varsigma)$ in Equation (9):

$$T_{2,f}^{G,\gamma}(t, \varsigma) = \frac{1}{G^*(0)} \int_{\{t, |V_F^G| > \gamma\}} V_f^G(\mu, \varsigma) \delta(t - \hat{v}_f^{[2]}(\mu, \varsigma)) d\mu \quad (16)$$

where γ is the threshold.

Meanwhile, the original signal $f(t)$ can be reconstructed by an inverse Fourier transform,

$$f(t) = F^{-1} \left(\int_{-\infty}^{+\infty} T_{2,f}^{G,\gamma}(t, \varsigma) dt \right) \quad (17)$$

where $F^{-1}(\bullet)$ represents the inverse Fourier transform.

3. Synthetic Example

In this section, we consider a synthetic multicomponent signal composed of two impulses at 0.015 s and 0.04 s and one chirp and one modulation sinusoid between 0.06 s and 0.5 s, as shown in Figure 1a, to illustrate the improvements brought by frequency-domain SST in comparison with the traditional STFT and FSST methods. The TFRs provided by STFT, FSST, FDSST, and FDSST2 are displayed in Figure 2a–d. It can be seen that STFT suffers from a poor time–frequency resolution owing to its fixed window function. FSST performs better than STFT since it squeezes the time–frequency coefficients in the frequency direction; however, the frequency squeezing also leads to time–frequency energy diffusion in time. FDSST is characterized by better time localization compared with the STFT and FSST methods, but it has relatively poor frequency resolution. The FDSST2 result clearly illustrates its improvement over FDSST for representing the whole signal. The resolutions in both time and frequency are greatly improved.

In order to obviously compare the performance of the above-mentioned approaches, we enlarged some areas indicated by two colored rectangle boxes in Figure 2; the results are depicted in Figures 3 and 4, respectively. For two impulse signals, the chirp signal and the sinusoid signal, the STFT exhibits poor time–frequency resolution (Figures 3a and 4a). The FSST provides a relatively nice TFR with a higher-frequency resolution (Figure 4b). However, for the signals with a strongly varying IF, both STFT and FSST fail to give the desired result. Compared with the STFT and FSST methods, FDSST can more effectively characterize the time attribute of the signal (Figure 3c). Furthermore, one can clearly see the advantage of FDSST2 in enhancing the energy concentration along the time direction (Figure 3d), which is more helpful for the feature extraction of strong frequency-modulated signals.

In addition, to illustrate FDSST’s and FDSST2’s robustness with respect to noise, we generated a series of noisy signals with signal-to-noise ratios (SNRs) ranging from 0 to 30 dB. Figure 1b shows the signal with an SNR of 4 dB. The resulting TFRs of applying the STFT, FSST, FDSST, and FDSST2 methods are displayed in Figure 5, and the enlarged TFR results marked by two rectangle boxes are depicted in Figures 6 and 7. As can be seen, the STFT is prone to being affected by noise, which blurs the TFR. In the result of FSST,

the noise enables time–frequency energy to spread around the ridge (Figure 7b), and as a result, the IF cannot be accurately estimated. By contrast, FDSST and FDSST2 have better anti-noise ability, especially the FDSST2. It can still show good energy concentration in the presence of noise (Figures 6d and 7d) where the local characteristics of the signal can be described well.

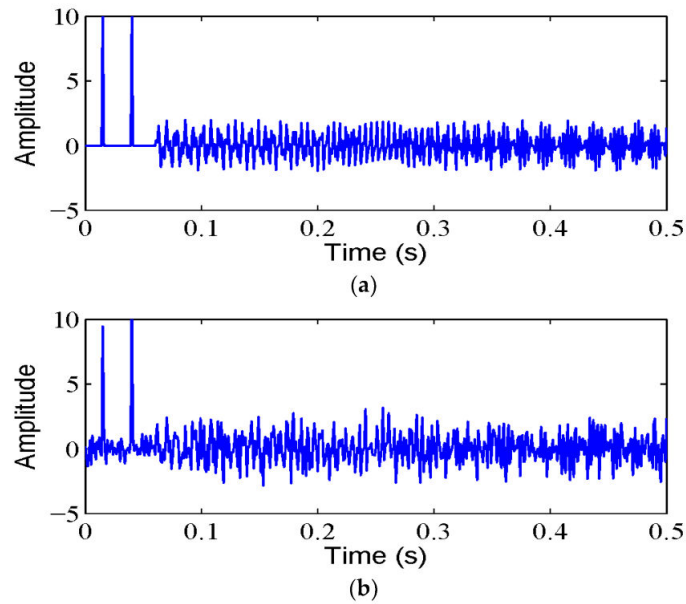


Figure 1. A synthetic signal (a) and noisy signal with an SNR of 4 dB (b).

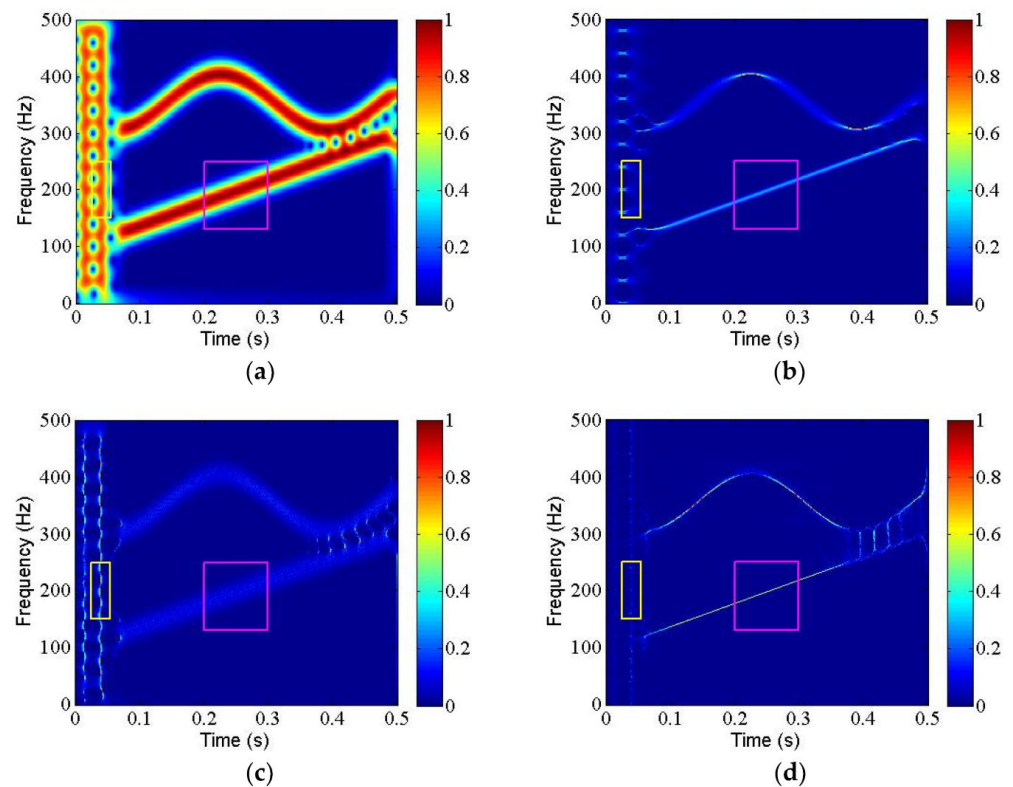


Figure 2. TFR results of the synthetic signal (Figure 1a). (a) STFT, (b) FSST, (c) FDSST, and (d) FDSST2. FDSST2 produces a highly energy-concentrated TFR.

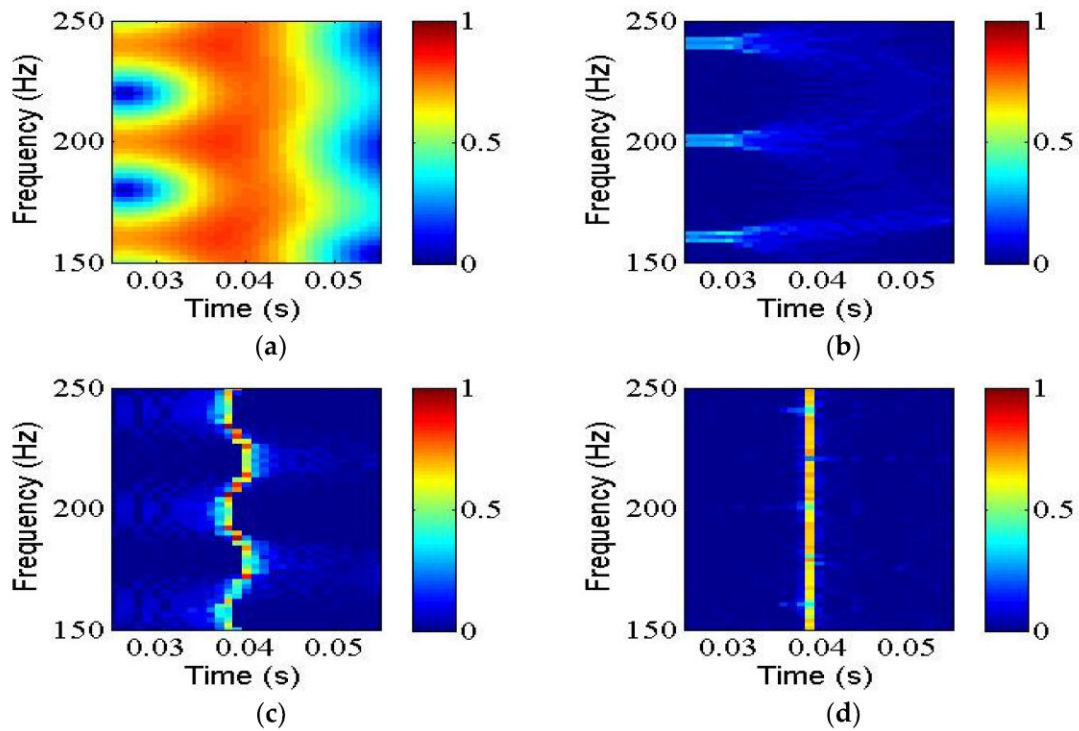


Figure 3. Enlarged TFR results from the yellow rectangle box in Figure 2. (a) STFT, (b) FSST, (c) FDSST, and (d) FDSST2. The FDSST2 has better time localization.

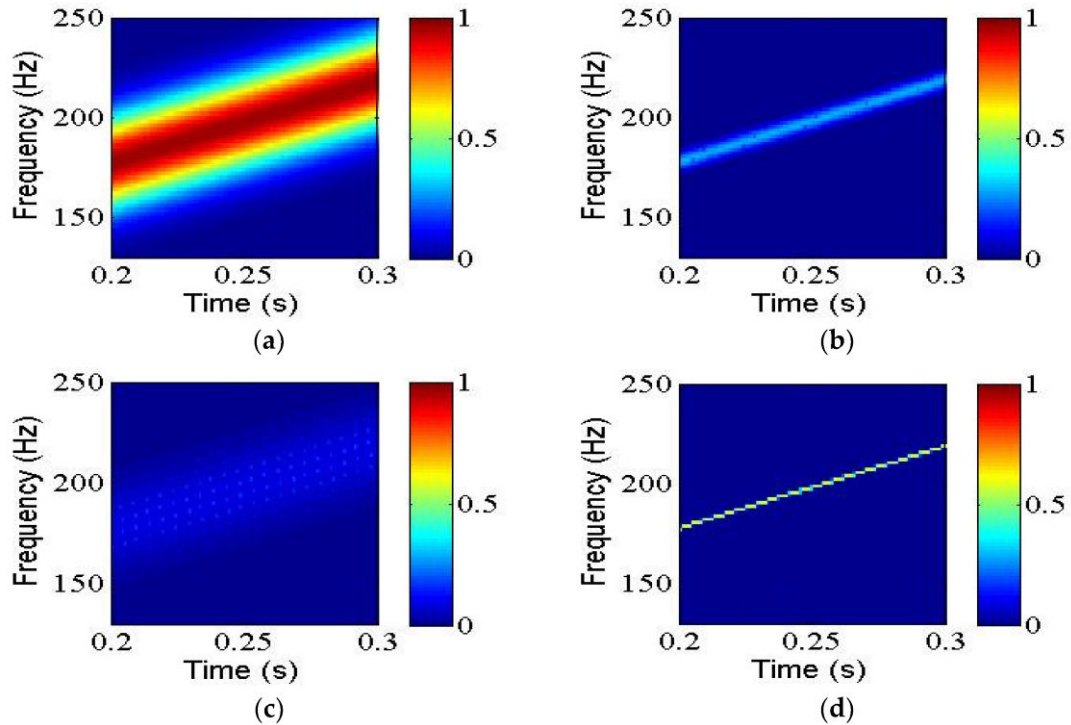


Figure 4. Enlarged TFR results from the magenta rectangle box in Figure 2. (a) STFT, (b) FSST, (c) FDSST, and (d) FDSST2. The FDSST2 is characterized by high-frequency resolution.

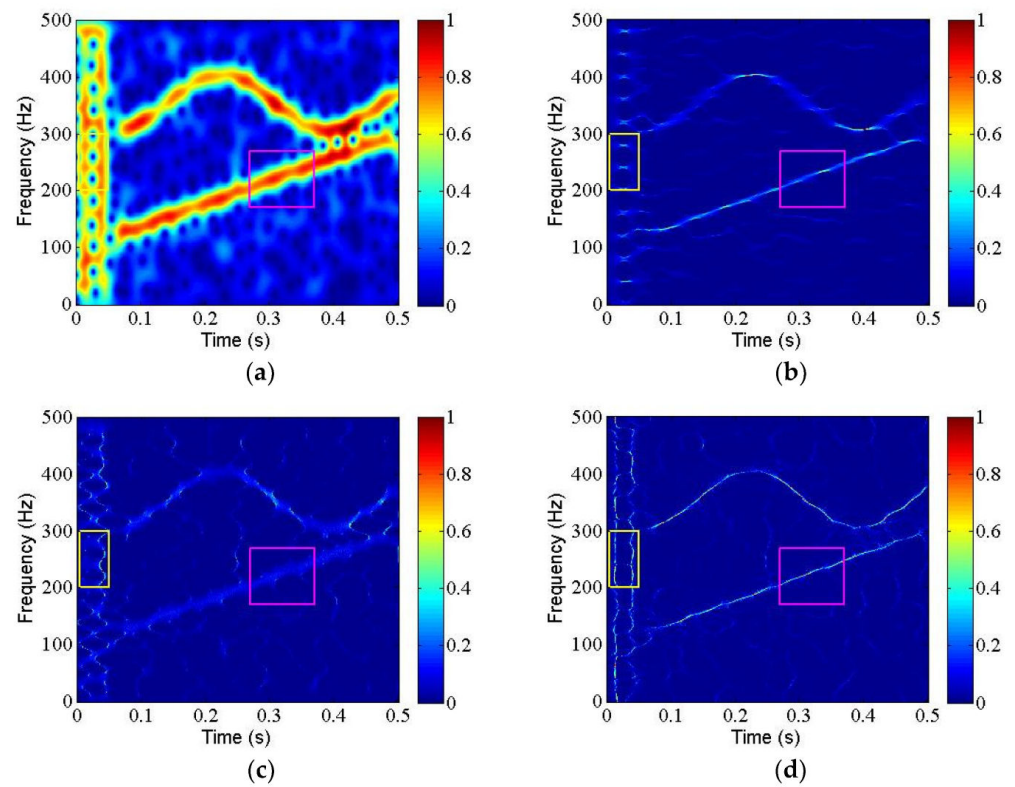


Figure 5. TFR results of the noisy synthetic signal (Figure 1b). (a) STFT, (b) FSST, (c) FDSST, and (d) FDSST2. The FDSST2 shows the better energy concentration in the presence of noise.

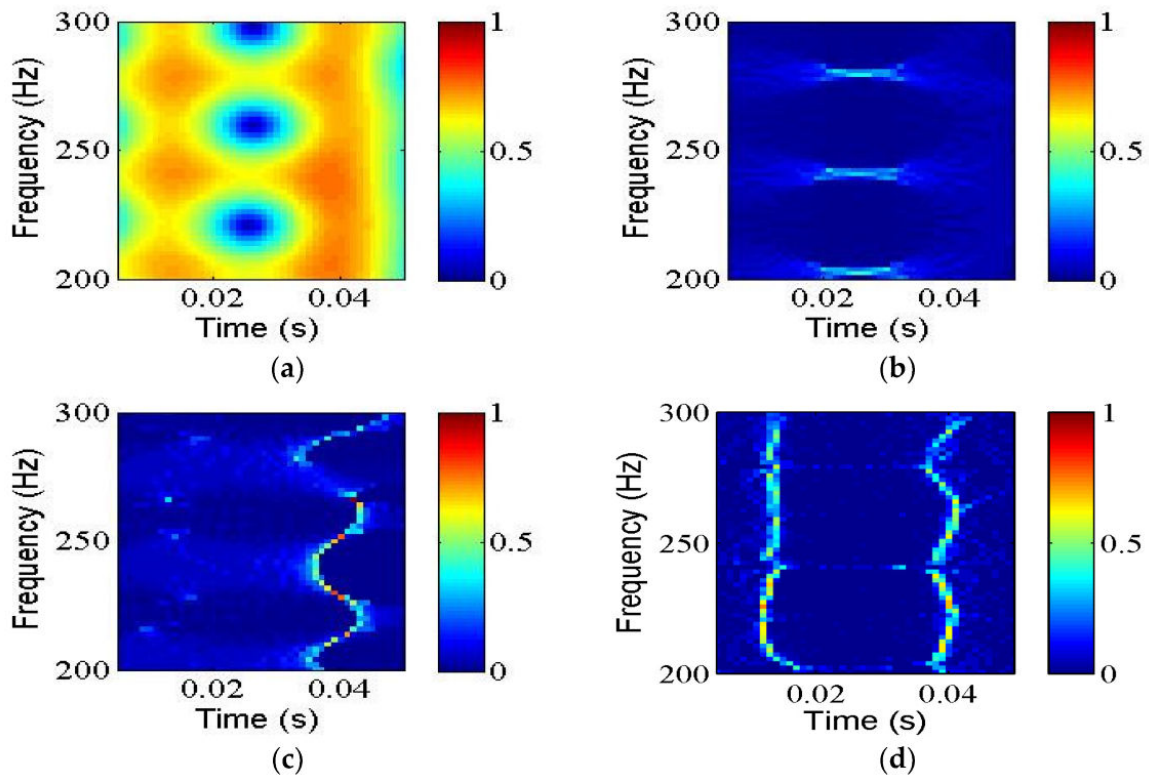


Figure 6. Enlarged TFR results from the yellow rectangle box in Figure 5. (a) STFT, (b) FSST, (c) FDSST, and (d) FDSST2. FDSST2 still shows the better time localization in the presence of noise.

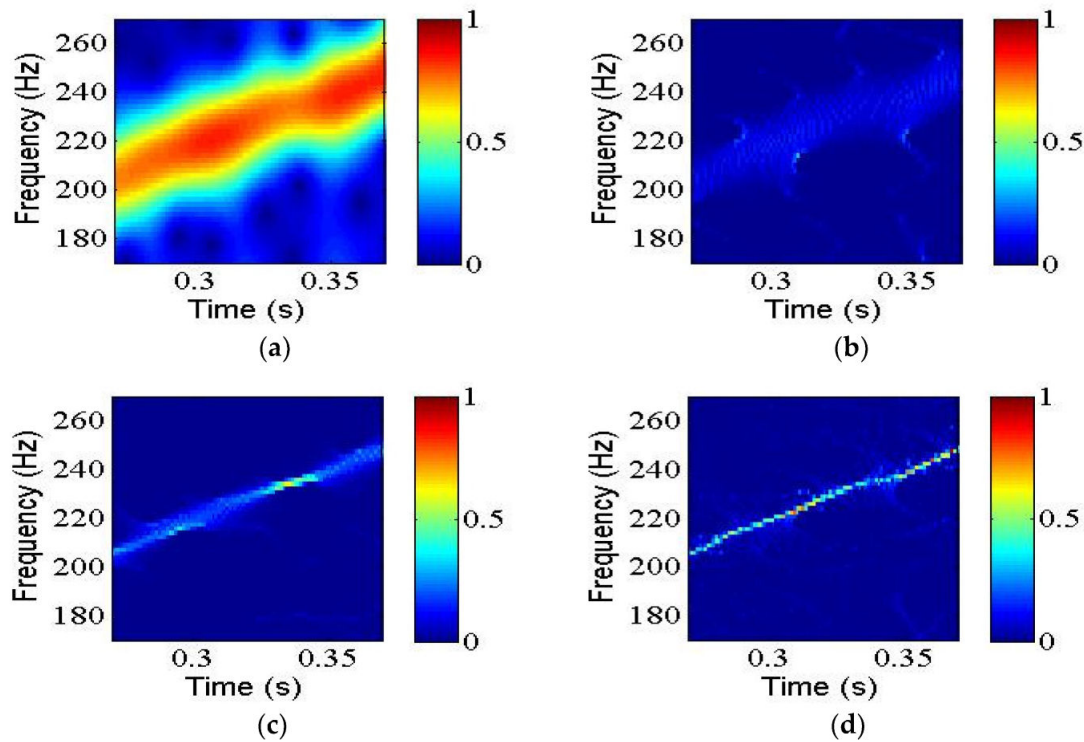


Figure 7. Enlarged TFR results from the magenta rectangle box in Figure 5. (a) STFT, (b) FSST, (c) FDSST, and (d) FDSST2. FDSST and FDSST2 have the better anti-noise abilities, especially FDSST2.

Finally, the Renyi entropy is employed to evaluate the performances of the STFT, FSST, FDSST, and FDSST2 methods. It is worth noting that a lower Renyi entropy means a more energy-concentrated TFR [27,28]. As shown in Figure 8, for the STFT, the value of the Renyi entropy is higher. The FSST and FDSST are almost equivalent in value of Renyi entropy. The FDSST2 has the lowest Renyi entropy; in other words, it can produce the most energy-concentrated TFR. The Renyi entropy is defined by

$$I = -\frac{1}{2} \log_2 \left(\frac{\iint_{R^2} |T(t, \zeta)|^3 d\zeta dt}{\iint_{R^2} |T(t, \zeta)| d\zeta dt} \right) \tag{18}$$

where $T(t, \zeta)$ denotes the TFR result.

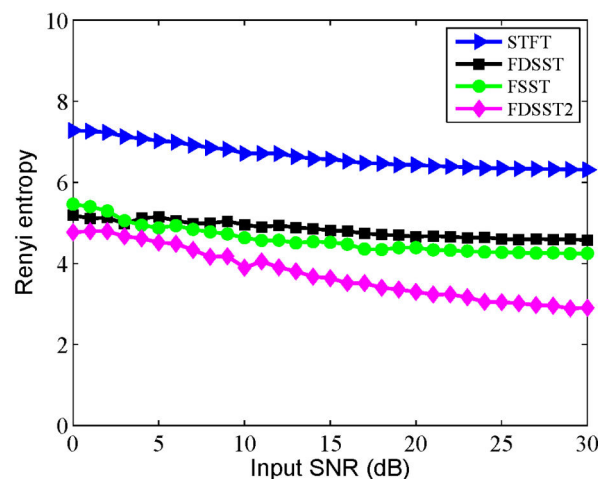


Figure 8. Renyi entropies of the TFRs from different TFA methods under different noise levels. FDSST2 has the lowest Renyi entropy in each noise level.

4. Real Example

To further illustrate the potential of frequency-domain SST in field data analysis, we employed real seismic data from a seismic land survey (Figure 9a), which was analyzed previously by Chen and Fomel [4] and Liu et al. [29]. These data are composed of 150 traces with 500 samples per trace and a sampling interval of 2 ms. First, a seismic trace labeled 120 (Figure 9b) was taken as an example to show the TFR results from the STFT, FSST, FDSST, and FDSST2 methods, which are depicted in Figure 10, and the enlarged local area indicated by a yellow rectangle box is shown in Figure 11. The STFT result indicates that there are four obvious spectral energies at 0.08 s, 0.15 s, 0.32 s, and 0.75 s, which correspond to the four strong amplitudes in the waveform (Figure 9b). However, the STFT is unable to effectively identify the time of occurrence due to the low time–frequency resolution (Figure 10a). The other methods, FSST, FDSST, and FDSST2, exhibit sparser representations in the time–frequency plane. It should be noted that the spectral energy of FSST diffuses along the time direction since the time–frequency coefficients are squeezed in frequency, which makes the time localization of FSST poor (Figures 10b and 11b). In the results of FDSST and FDSST2, the time–frequency energy is concentrated in time (Figure 10c,d). In this sense, FDSST and FDSST2 are more helpful for detecting these existing spectral energies and thus facilitating seismic interpretation. In particular, FDSST2 more clearly characterizes the time of these spectral energies (Figures 10d and 11d), which is due to the second-order local modulation operator.

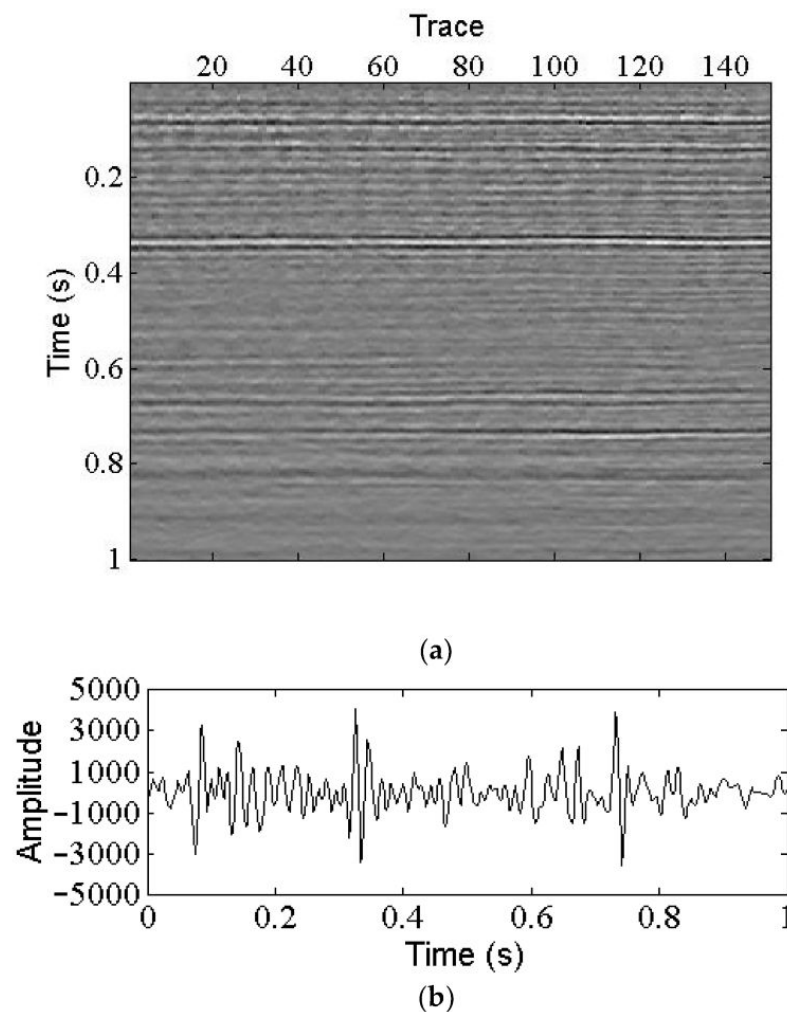


Figure 9. A field data (a) and trace 120 (b).

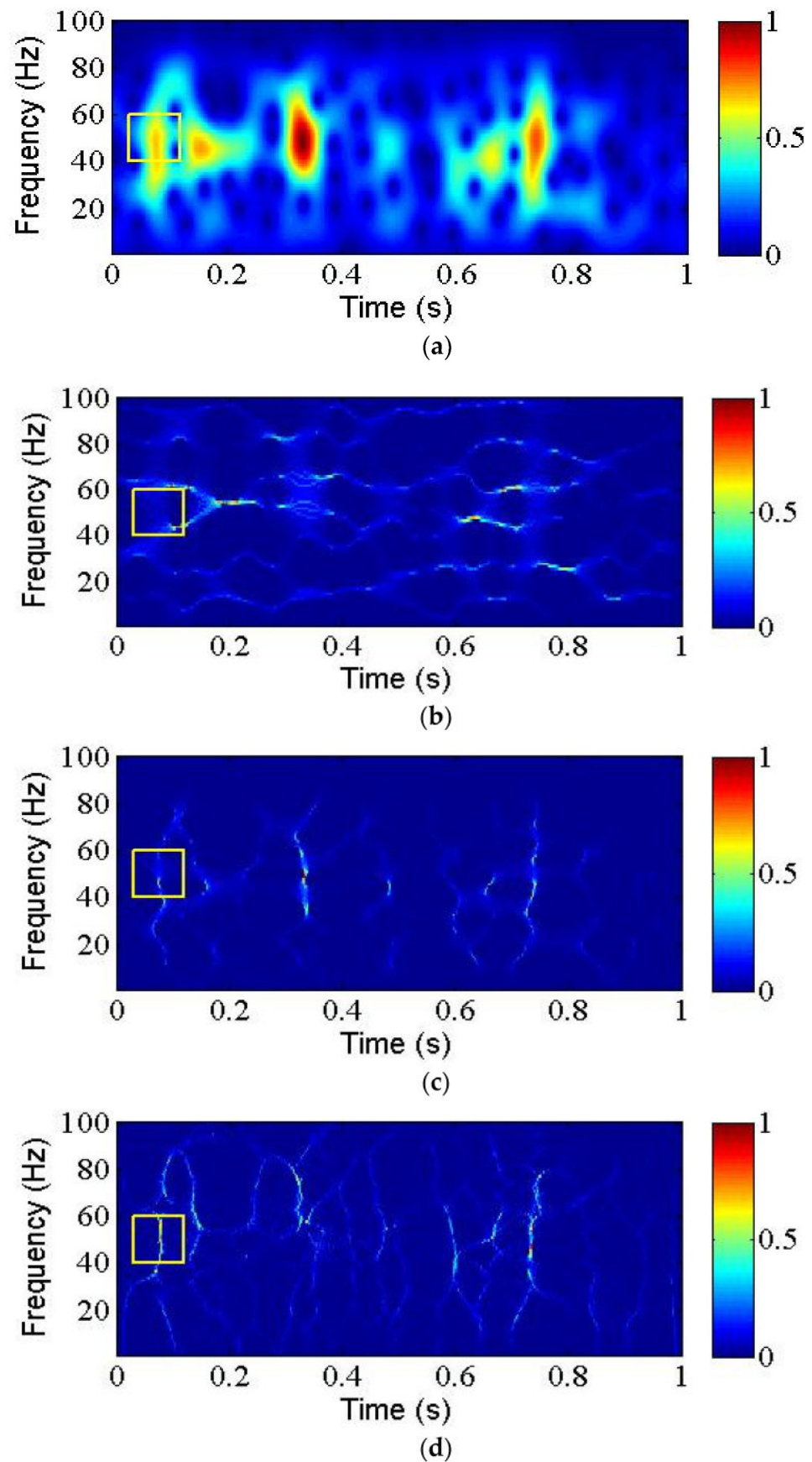


Figure 10. The TFR results of trace 120 obtained by (a) STFT, (b) FSST, (c) FDSST, and (d) FDSST2.

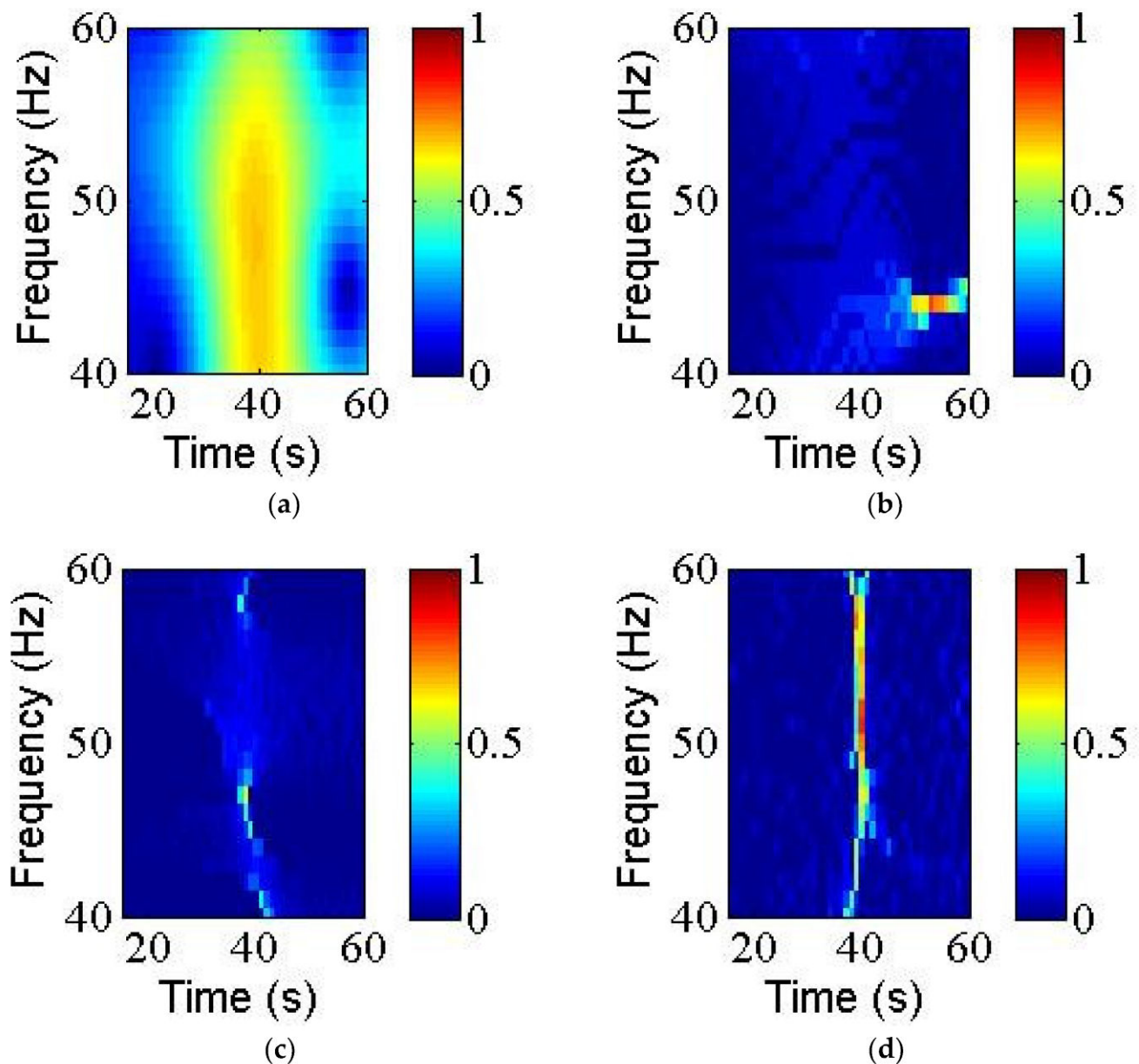


Figure 11. Enlarged local TFR results corresponding to Figure 10 for (a) STFT, (b) FSST, (c) FDSST, and (d) FDSST2. FDSST2 generates the more energy-concentrated TFR.

Next, we extracted 40 Hz frequency slices based on the results of the STFT, FSST, FDSST and FDSST2 methods, which are displayed in Figure 12. Figure 13 is the enlarged local area from a white rectangle box in Figure 12. The STFT fails to effectively provide stratigraphic information due to the impact of the time–frequency resolution (Figures 12a and 13a). FSST improves the frequency resolution to a certain extent, but it is not an ideal result (Figures 12b and 13b). FDSST and FDSST2 provide much sparser representations and depict the spectral characteristics of seismic reflections more clearly (Figure 12c,d). Compared to the results of FDSST, FDSST2 performs better, with more continuous reflections and more detailed stratifications (Figures 12d and 13d).

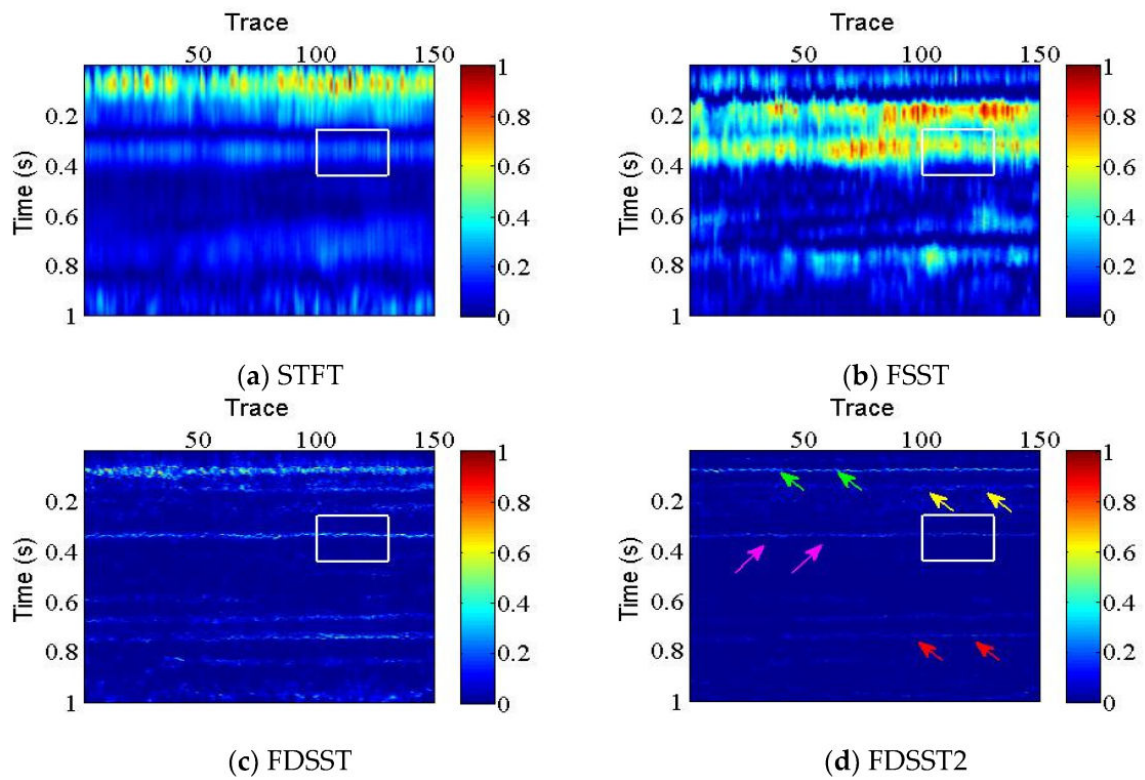


Figure 12. Representation of 40 Hz frequency slices using STFT-based method (a), FSST-based method (b), FDSST-based method (c), and FDSST2-based method (d). FDSST2 shows a higher time resolution.

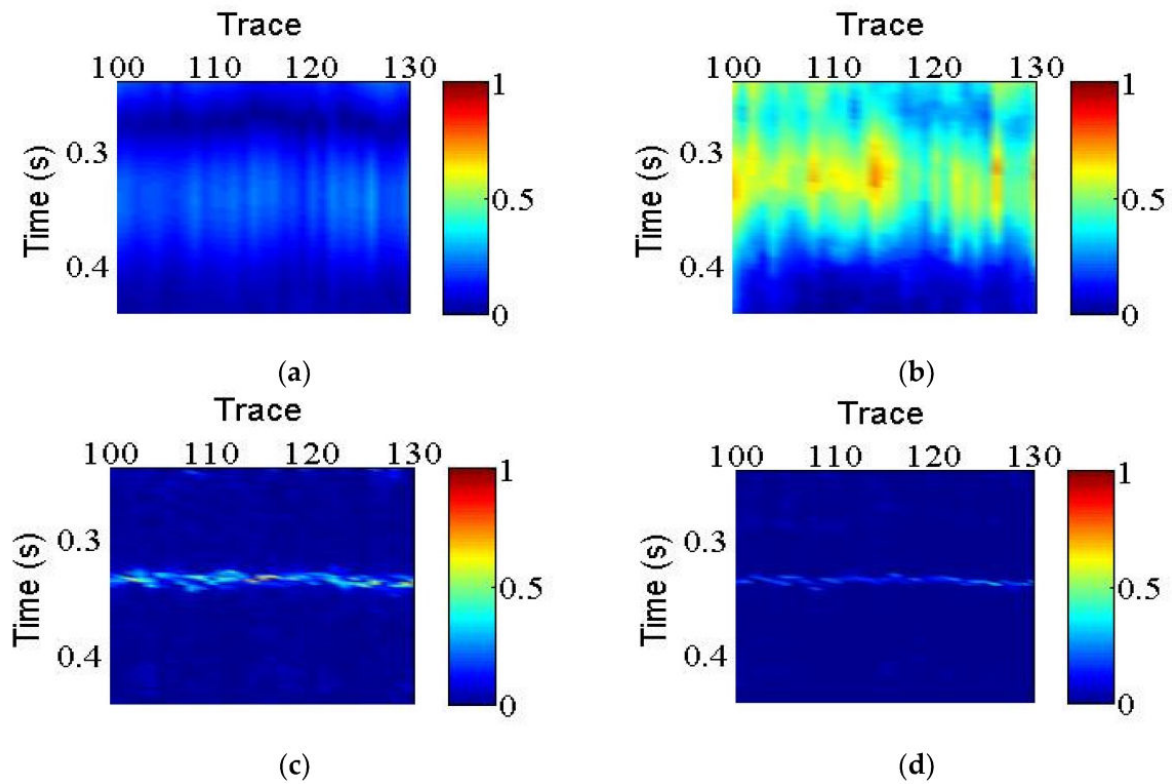


Figure 13. Enlarged local TFR results corresponding to Figure 12. (a) STFT, (b) FSST, (c) FDSST, and (d) FDSST2.

5. Discussion

TFA is one of the most effective tools for characterizing nonstationary signals. STFT analyzes the frequency content of a signal over time, and it is based on a fixed widow, which means that high time resolution and frequency resolution cannot be obtained simultaneously. FSST is a kind of reassignment method that aims to sharpen a TFR by reassigning the time–frequency coefficients of STFT in the frequency direction. FDSST and FDSST2 utilize a frequency-domain Gaussian modulated linear chirp model to achieve the TFRs, where the amplitude is locally approximated by a Gaussian function, and the phase is a quadratic polynomial. Specifically, in the FDSST algorithm, the reassignment operation is implemented in the time direction rather than the frequency direction, as is the case with FSST. Meanwhile, the IF is replaced by a GD estimator in the reassignment operation. Subsequently, we extended the FDSST to a second-order version, namely FDSST2, using a second-order local modulation operator and a second-order local GD estimation. Thus, both FDSST and FDSST2 are more suitable for describing the signals characterized by a rapidly changing IF.

Due to the Heisenberg uncertainty principle, the time–frequency resolution of STFT is poor, which limits the wide application of such a technique to some extent. FSST integrates STFT and the ‘synchrosqueezing’ idea. In the FSST method, the IF estimator is utilized to sharpen the STFT representation of the signal in the frequency direction. However, the hypothesis of weak frequency modulation for the modes making up the signal makes the FSST unsuitable for analyzing some nonstationary signals, such as signals with strongly varying IF and even impulse signals. In this study, we employ a frequency-domain Gaussian-modulated linear chirp model to deduce the SST. Next, the GD with respect to frequency is utilized to depict the ridge. Then, we define a local modulation operator to rearrange the time–frequency coefficients along the time direction. Since the proposed method is implemented based on STFT in the frequency domain, it is thus called frequency-domain SST. Inspired by FSST2, we introduce a second-order local modulation operator and drive the frequency-domain second-order SST (FDSST2). FDSST and FDSST2 achieve relatively highly energy-concentrated TFR for signals with strongly varying IF, especially FDSST2. In fact, the frequency-domain SST and FSST are two complementary methods. The FSST is suitable for characterizing a slowly time-varying signal, while the frequency-domain SST is more capable of a strongly time-varying signal. Both methods have their own advantages and working conditions. In addition, we also evaluate the computation costs of the STFT, FSST, FDSST and FDSST2 methods based on synthetic signal and field data, which are listed in Table 1. It can be clearly seen that STFT takes the shortest time, FSST and FDSST are nearly equivalent in time, and FDSST2 takes the longest time because it involves several STFTs compared to FDSST. All tests were conducted on a PC station with an Intel Pentium Duo Core CPU clocked at 2.53 GHz and 2 GB of RAM.

Table 1. Computational costs of STFT, FSST, FDSST and FDSST2.

Data	STFT	FSST	FDSST	FDSST2
Synthetic data	0.22 s	0.41 s	0.34 s	1.03 s
Field data	36.02 s	47.09 s	43.62 s	147.31 s

In the experiments, we show that the proposed FDSST and FDSST2 methods clearly outperform STFT and FSST with regard to energy concentration and noise robustness. Further, we will apply our method to more complicated signals. However, the FDSST2 has a high computational burden because the algorithm itself needs to perform multiple STFTs. Generally, a computationally efficient algorithm is favorable in practical applications. Therefore, future work will focus on parallel algorithm development to reduce the computational burden.

The Renyi entropy is a common measure to estimate the distribution concentration of a TFR. The larger the Renyi entropy is, the less concentrated the TFR is [27]. Considering the

readability of the TFR, we utilize the Renyi entropy to evaluate the energy concentration of the TFRs obtained by the STFT, FSST, FDSST and FDSST2 methods. In the paper, the 3-order Renyi entropy is used to quantitatively measure the time–frequency energy concentration since it uses the smallest integer value to yield a well-defined useful information measure for a large class of signals [30].

Finally, we summarize a list of abbreviations of some technical terms frequently used in the paper, which is shown in Table 2.

Table 2. List of abbreviations.

Abbreviation	Full Name
SST	Synchrosqueezing transform
IF	Instantaneous frequency
GD	Group delay
TFA	Time–frequency analysis
STFT	Short-time fourier transform
FSST	STFT-based SST
CWT	Continuous wavelet transform
TFR	Time–frequency representation
WVD	Wigner–Ville distribution
RM	Reassignment method
FSST2	Second-order SST
FSSTN	N-order SST
TPST	Three-parameter S transform
TSET	Time-synchroextracting transform
TSST	Time-reassigned synchrosqueezing transform
FDSST	Frequency-domain SST
FDSST2	Frequency-domain second-order SST
SNR	Signal-to-noise ratio

6. Conclusions

In this paper, a new frequency-domain synchrosqueezing transform is presented for seismic time–frequency analysis. We derive FDSST and FDSST2 using a frequency-domain Gaussian-modulated linear chirp model. The FDSST and FDSST2 methods achieve a highly energy-concentrated TFR for signals with strongly varying IF, especially for FDSST2. In the proposed algorithm, the GD estimation rather than the IF estimator is utilized to calculate the ridge. Meanwhile, a new synchrosqueezing operator is implemented to rearrange the time–frequency energy along the time direction. The effectiveness of FDSST and FDSST2 is validated using the synthetic signal and field dataset. Both methods provide superior results over some classical TFA techniques, such as STFT and FSST, and are much more robust to noise. Moreover, we quantitatively evaluate the performance of the FDSST and FDSST2 methods using Renyi entropy and SNR. The results indicate that the FDSST2 has the lowest Renyi entry and the strongest robustness to noise compared with the STFT and FSST methods. A real example further indicates the potential of frequency-domain SST in the delineation of subsurface geological structures, which renders this technique promising for seismic data analysis. Future work will be devoted to the influence of noise on the reassignment operators and parallel algorithm development.

Author Contributions: Conceptualization, P.B. and W.L.; methodology, P.B.; software, H.Z.; validation, H.Z.; formal analysis, L.Z.; investigation, G.Z.; resources, L.Z.; data curation, G.Z.; writing—original draft preparation, W.L.; writing—review and editing, J.Z.; visualization, W.L.; supervision, B.H. project administration, B.H.; funding acquisition, P.B. All authors have read and agreed to the published version of the manuscript.

Funding: This research was funded by the project of ESI Discipline Construction of Changsha Medical University [2022CYY018], the project of the Hunan Provincial Education Commission Foundation [22C0669] and the project of the Hunan Provincial Health Commission Foundation [D202302088596].

Data Availability Statement: The data used to support the finds of this study are available from the corresponding author upon request.

Conflicts of Interest: The authors declare no conflict of interest.

Appendix A

The proof of Equation (3) is as follows:

The window function g can be expressed as

$$g(t) = \frac{1}{2\pi} \int_{-\infty}^{+\infty} G(\zeta) e^{i2\pi\zeta t} d\zeta \tag{A1}$$

Then, the frequency-domain STFT can be written as

$$\begin{aligned} V_f^g(t, \zeta) &= V_f^G(t, \zeta) \\ &= \int_{-\infty}^{+\infty} f(\tau) g^*(\tau - t) e^{-i2\pi\zeta\tau} d\tau \\ &= \int_{-\infty}^{+\infty} f(\tau) \left(\frac{1}{2\pi} \int_{-\infty}^{+\infty} G^*(\xi) e^{-i2\pi\xi(\tau - t)} d\xi \right) e^{-i2\pi\zeta\tau} d\tau \\ &= \frac{1}{2\pi} \int_{-\infty}^{+\infty} G^*(\xi) e^{i2\pi\xi t} \left(\int_{-\infty}^{+\infty} f(\tau) e^{-i2\pi(\xi + \zeta)\tau} d\tau \right) d\xi \\ &= \frac{1}{2\pi} \int_{-\infty}^{+\infty} G^*(\xi) e^{i2\pi\xi t} F(\xi + \zeta) d\xi \\ &= \frac{1}{2\pi} \int_{-\infty}^{+\infty} F(\xi) G^*(\xi - \zeta) e^{i2\pi t(\xi - \zeta)} d\xi \end{aligned} \tag{A2}$$

Appendix B

The proof of Equation (4) is as follows:

$$\begin{aligned} &F^{-1} \left(\frac{1}{G^*(0)} \int_{-\infty}^{+\infty} V_f^G dt \right) \\ &= F^{-1} \left(\frac{1}{G^*(0)} \int_{-\infty}^{+\infty} \int_{-\infty}^{+\infty} f(\tau) g^*(\tau - t) e^{-i2\pi\zeta\tau} d\tau dt \right) \\ &= F^{-1} \left(\int_{-\infty}^{+\infty} \left[\frac{1}{G^*(0)} \int_{-\infty}^{+\infty} g(\tau - t) dt \right]^* f(\tau) e^{-i2\pi\zeta\tau} d\tau \right) \\ &= F^{-1} (f(\tau) e^{-i2\pi\zeta\tau} d\tau) \\ &= f(t) \end{aligned} \tag{A3}$$

References

1. Castagna, J.P.; Sun, S.; Siegfried, R.W. Instantaneous spectral analysis: Detection of low-frequency shadows associated with hydrocarbons. *Lead. Edge* **2003**, *22*, 120–127. [\[CrossRef\]](#)
2. Liu, Y.; Fomel, S. Seismic data analysis using local time-frequency decomposition. *Geophys. Prospect.* **2013**, *61*, 516–525. [\[CrossRef\]](#)
3. Xue, Y.; Cao, J.; Wang, D.; Du, H.; Yao, Y. Application of the variational-mode decomposition for seismic time-frequency analysis. *IEEE J. Sel. Top. Appl. Earth Obs. Remote Sens.* **2016**, *9*, 3821–3831. [\[CrossRef\]](#)
4. Chen, Y.; Fomel, S. Random noise attenuation using local signal and noise orthogonalization. *Geophysics* **2015**, *80*, WD1–WD9. [\[CrossRef\]](#)
5. Liu, W.; Liu, Y.; Li, S.; Chen, Y. A review of variational mode decomposition in seismic data analysis. *Surv. Geophys.* **2023**, *44*, 323–355. [\[CrossRef\]](#)
6. Wang, P.; Gao, J.; Wang, Z. Time-frequency analysis of seismic data using synchrosqueezing transform. *IEEE Geosci. Remote Sens. Lett.* **2014**, *11*, 2042–2044. [\[CrossRef\]](#)
7. Allen, J.B. Short term spectral analysis, synthetic and modification by discrete Fourier transform. *IEEE Trans. Acoust. Speech Signal Process.* **1977**, *25*, 235–238. [\[CrossRef\]](#)

8. Sinha, S.; Routh, P.; Anno, P.; Castagna, J. Spectral decomposition of seismic data with continuous-wavelet transform. *Geophysics* **2005**, *70*, 19–25. [[CrossRef](#)]
9. Yuan, S.; Shi, P.; Jing, Z.; Gao, J.; Wang, S. Sparse Bayesian learning-based seismic high-resolution time-frequency analysis. *IEEE Geosci. Remote Sens. Lett.* **2019**, *16*, 623–627. [[CrossRef](#)]
10. Li, F.; Wu, B.; Liu, N.; Hu, Y.; Wu, H. Seismic time-frequency analysis via adaptive mode separation-based wavelet transform. *IEEE Geosci. Remote Sens. Lett.* **2020**, *17*, 696–700. [[CrossRef](#)]
11. Liu, W.; Liu, Y.; Li, S. Demodulated multisynchrosqueezing S transform for fault diagnosis of rotating machinery. *IEEE Sens. J.* **2022**, *22*, 20773–20784. [[CrossRef](#)]
12. Cohen, L. Time-Frequency Distribution—A Review. *Proc. IEEE* **1989**, *77*, 941–981. [[CrossRef](#)]
13. Auger, F.; Flandrin, P. Improving the readability of time-frequency and time-scale representations by the reassignment method. *IEEE Trans. Signal Process.* **1995**, *43*, 1068–1089. [[CrossRef](#)]
14. Daubechies, I.; Lu, J.; Wu, H.-T. Synchrosqueezed wavelet transform: An empirical mode decomposition-like tool. *Appl. Comput. Harmon. Anal.* **2011**, *30*, 243–261. [[CrossRef](#)]
15. Daubechies, I.; Maes, S. *A Nonlinear Squeezing of the Continuous Wavelet Transform Based on Auditory Nerve Models Wavelets in Medicine and Biology*; CRC Press: Boca Raton, FL, USA, 1996; pp. 527–546.
16. Herrera, R.H.; Han, J.; van der Baan, M. Applications of the synchrosqueezing transform in seismic time-frequency analysis. *Geophysics* **2014**, *79*, V55–V64. [[CrossRef](#)]
17. Liu, W.; Liu, Y.; Li, S. Demodulated synchrosqueezing S transform and its application to machine fault diagnosis. *Meas. Sci. Technol.* **2023**, *34*, 065004. [[CrossRef](#)]
18. Thakur, G.; Wu, H.-T. Synchrosqueezing-based recovery of instantaneous frequency from nonuniform samples. *SIAM J. Math. Anal.* **2011**, *43*, 2078–2095. [[CrossRef](#)]
19. Oberlin, T.; Meignen, S.; Perrier, V. Second-order synchrosqueezing transform or invertible reassignment? Towards ideal time-frequency representations. *IEEE Trans. Signal Process.* **2015**, *63*, 1335–1344. [[CrossRef](#)]
20. Pham, D.-H.; Meignen, S. High-order synchrosqueezing transform for multicomponent signals analysis—With an application to gravitational-wave signal. *IEEE Trans. Signal Process.* **2017**, *65*, 3168–3178. [[CrossRef](#)]
21. Liu, W.; Liu, Y.; Li, S.; Chen, W. Adaptive time-reassigned synchrosqueezing transform for bearing fault diagnosis. *IEEE Sens. J.* **2023**, *23*, 8545–8555. [[CrossRef](#)]
22. Liu, N.; Gao, J.; Zhang, B.; Li, F.; Wang, Q. Time-frequency analysis of seismic data using a three parameters S transform. *IEEE Geosci. Remote Sens. Lett.* **2018**, *15*, 142–146. [[CrossRef](#)]
23. Li, Z.; Gao, J.; Wang, Z. A time-synchroextracting transform for the time-frequency analysis of seismic data. *IEEE Geosci. Remote Sens. Lett.* **2020**, *17*, 864–868. [[CrossRef](#)]
24. Bing, P.; Liu, W.; Liu, Y. Seismic time-frequency analysis based on time-reassigned synchrosqueezing transform. *IEEE Access* **2021**, *9*, 133686–133693. [[CrossRef](#)]
25. Yu, C.; Wang, S.; Cheng, L. Application of high-resolution processing in seismic data based on an improved synchrosqueezing transform. *Front. Earth Sci.* **2022**, *10*, 956817. [[CrossRef](#)]
26. Paksima, S.; Radad, M.; Roshandel Kahoo, A.; Soleimani Monfared, M. Identification of thin gas reservoir in reflection seismic data by synchrosqueezing S-transform in time-frequency representation. *Arab. J. Geosci.* **2023**, *16*, 376–387. [[CrossRef](#)]
27. Sheu, Y.; Hsu, L.; Chou, P.; Wu, H. Entropy-based time-varying window width selection for nonlinear-type time-frequency analysis. *Int. J. Data Sci. Anal.* **2017**, *3*, 231–245. [[CrossRef](#)]
28. Stankovic, L. A measure of some time-frequency distributions concentration. *Signal Process.* **2001**, *81*, 621–631. [[CrossRef](#)]
29. Liu, W.; Cao, S.; Chen, Y. Applications of variational mode decomposition in seismic time-frequency analysis. *Geophysics* **2016**, *81*, V365–V378. [[CrossRef](#)]
30. Wang, S.; Chen, X.; Tong, C.; Zhao, Z. Matching synchrosqueezing wavelet transform and application to aeroengine vibration monitoring. *IEEE Trans. Instrum. Meas.* **2017**, *66*, 360–372. [[CrossRef](#)]

Disclaimer/Publisher’s Note: The statements, opinions and data contained in all publications are solely those of the individual author(s) and contributor(s) and not of MDPI and/or the editor(s). MDPI and/or the editor(s) disclaim responsibility for any injury to people or property resulting from any ideas, methods, instructions or products referred to in the content.